Acta Astronautica 170 (2020) 154–162

Contents lists available at ScienceDirect

Acta Astronautica

journal homepage: www.elsevier.com/locate/actaastro

Research paper

A model for macro-performances applied to low power coaxial pulsed plasma thrusters

Hang Li[a], Zhiwen Wu[a,*], Guorui Sun[b], Kangwu Zhu[c], Tiankun Huang[a], Xiangyang Liu[a], William Yeong Liang Ling[a], Ningfei Wang[a]

[a] School of Aerospace Engineering, Beijing Institute of Technology, Beijing, 100081, PR China
[b] Tianjin Institute of Power Sources, Tianjin, 300384, PR China
[c] Shanghai Aerospace Control Technology Institute, Shanghai, 201109, PR China

ARTICLE INFO

Keywords:
Coaxial pulsed plasma thruster
Model simulation
Macro-performances estimation

ABSTRACT

Pulsed plasma thrusters (PPT), as an important developing direction of micro-satellite propulsion system, are attracting more and more attention. Low power coaxial PPT has great advantages in miniaturization because of its coaxial structure, which is beneficial for micro-satellite applications. Since there are few macro-performances estimation model in low power coaxial PPT, this paper establishes a model based on one-dimensional electromechanical PPT model and gas dynamic pressure forces model to describe macro-performances of low power coaxial PPT. In this model, the electromechanical model describes the plasma electromagnetic acceleration process, current and voltage changes of the main circuit during the discharge process, and the gas dynamic pressure forces model describes the expansion and acceleration of the neutral gas group in the discharge channel. To verify the model, we compared the voltage and current obtained from model simulation with the experimental results, and compared the impulse bit measured in the experiment with the impulse bit calculated by the model. The results show that the model established in this paper can well simulate the variation of voltage and current during the working process of low power coaxial PPT, and can preliminarily estimate the macro performances of the thruster.

1. Introduction

Pulsed plasma thruster (PPT), which was first applied on Zond 2 spacecraft in 1964, is one of the promising electric propulsion devices. PPT has the characteristics [1–4] of high specific impulse, light weight and simple structure which can meet the requirements of a small satellite propulsion system [5,6]. Over several decades of development, it has been successfully applied to more than ten in-orbit propulsion missions [7,8], such as station-keeping, attitude control and orbit transfer [9,10].

In recent years, there has been a growing concern about electric propulsion devices due to a trend towards micro-satellites in the commercial and scientific areas [11]. Hall thrusters have the advantages of high specific impulse, long life and high efficiency, therefore, they have a broad application prospect in spacecraft attitude control, station-keeping, orbit transfer [12–15], etc. An ion thruster, on the other hand, consists of an ion source and a neutralizer, and both use an electron-cyclotron resonance heating to generate plasma and can perform the main propulsion task of a deep space detector [16,17]. Based on the vacuum arc thruster, George Washington University (GWU) has developed the Micro-Cathode Arc Thruster (μCAT), which is a high specific impulse (2000–3500s), solid metal fueled, low average power (< 0.1 W when operating) micro-thruster of small cross section (5 mm or less), with a mass of less than 200 g [18].

Compared with Hall thrusters and Ion thrusters, PPTs [19,20] have the advantages of simpler structure, stronger reliability and lighter weight. Furthermore, the storage and supply of propellant in Hall thrusters and Ion thrusters are much more complicated than those in PPTs [21,22]. Compared with μCAT, the impulse bit generated by PPT thruster is larger, which can meet the demand of larger thrust tasks. Moreover, the technology is mature and reliable after years of development. All of this makes PPT very suitable for micro-satellites.

In order to meet the needs of modern micro-satellite electric propulsion system, PPT has been gradually developing towards miniaturization in recent years. The low power coaxial PPT, as a kind of PPT, has great advantages in miniaturization because of its coaxial structure [23]. U.S. Air Force Institute of Technology has done a lot of research and experiments on the thruster for performance optimization, plume

* Corresponding author. Beijing Institute of Technology, PR China.
E-mail address: bitwzw@bit.edu.cn (Z. Wu).

https://doi.org/10.1016/j.actaastro.2019.11.014
Received 15 August 2019; Received in revised form 1 November 2019; Accepted 10 November 2019
Available online 16 November 2019

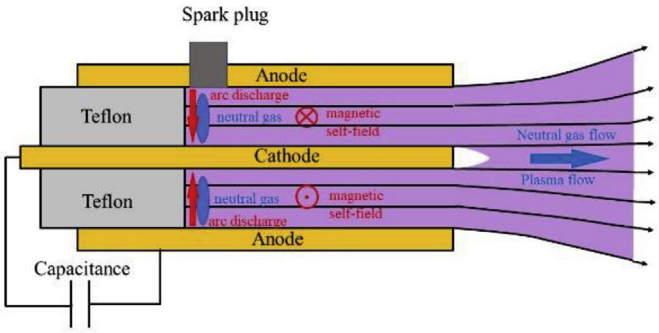

Fig. 1. Schematic of a coaxial PPT.

research and engineering application [24,25]. Compared with electrothermal coaxial thrusters, this low-power coaxial thruster is lighter in weight (no propellant supply) and smaller in size (spark plugs can be removed with a three-electrode structure).

A schematic of a coaxial PPT is shown in Fig. 1. The discharge of the main capacitor generates an electric arc, which ablates the propellant and produces a certain amount of neutral gas. Under the action of a strong electric field, a part of the neutral gas ionizes into a plasma group, which accelerates along the electrode discharge channel under the combined action of the electric field and the induced magnetic field in the discharge channel. And the unionized neutral gas group also accelerates under the action of thermal expansion. Due to the acceleration of the plasma and neutral gas, the thruster generates pulsed thrust.

When designing PPT, researchers usually use numerical models to estimate the performance of PPT in various design schemes, so as to select the best design scheme. At the same time, due to the extremely short working time of PPT (< 100 μs), it is difficult to conduct further research on the physical mechanism of PPT work process only by experimental means, so it is necessary to explore with the aid of numerical model. Over the past 50 years, PPT researchers have established various numerical models [26,27], with “slug” model being the most widely used model, which is mainly used to quickly estimate the thrust performance of PPT.

The “slug” model was first proposed by Jahn [28] to describe the working process of parallel plate electrode PPT. The model can simply predict macro-characteristics of a parallel plate electrode PPT, such as efficiency, impulse bit and specific impulse, and determine the parameters that affect the performance of PPT, providing guidance for the design of thruster. Waltz et al. [29] modified the original circuit equations with the energy conservation equation and extended the “slug” model to the LES PPT of Lincoln Laboratory. Leiweke [30] proposed a special “edge” inductance model that attempts to simulate the effects of finite parallel plates in the “slug” model to optimize the LES-8/9 PPT. Later, Demetriou et al. [31,32] proposed an electromechanical model, whose essence is still an improved form of “slug” model. They added a control item to the momentum equation of the "slug" model, which was set as an external magnetic field, and used to control the plasma velocity of the PPT in an open loop; Wagner et al. [33] developed “snowplow” or “slug” model for high-power (more than 10 kW) coaxial plasma accelerator to describe the electric discharge and plasma acceleration.

It can be seen that the previous” slug " model research mainly focused on parallel plate PPT, and the “snowplow” or “slug” model for coaxial plasma accelerator only considered the contribution of plasma acceleration to thrust which is only suitable for high-power thrusters. There are few related models for estimating the macro-performance of low power coaxial PPT(1–100 W), which need to consider the influence of aerodynamic force on the macro-performance of thruster.

In order to meet the urgent need of preliminary optimization design and test verification of a low power coaxial PPT prototype, it is necessary to establish a numerical model describing the working process of low power coaxial PPT to quickly estimate its thrust performance. In this paper, we establish a model to describe macro-performances of low power coaxial pulsed plasma thrusters based on one-dimensional electromechanical parallel plate PPT model and gas dynamic pressure forces model.

2. Model description

The model is based on electromechanical model [31,32] and gas dynamic pressure forces model [34]. The electromechanical model describes the plasma electromagnetic acceleration process and the current and voltage changes of the main circuit during the discharge process based on the one-dimensional electromechanical parallel plate PPT model. The gas dynamic pressure forces model describes the expansion and acceleration of the neutral gas group in the discharge channel. It can be divided into five parts: circuit model, magnetic field model, inductance model, plasma resistance model and dynamics model.

The following assumptions and methods are made to obtain a simple analytical model.

1) The electric circuit is theoretically idealized as a discrete, moveable LCR circuit model.
2) Kirchhoff's voltage and Faraday's law are used to describe the circuit of thruster.
3) Inductance and current are functions of time with all other parameters, while resistance remains constant over the acceleration process.
4) The plasma group is assumed to be a circular conducting sheet of uniform density [35]. The circuit geometry made up of electrodes and plasma sheet can be approximated as a spiral wound ring with a rectangular section
5) Acceleration effect of Lorentz force on plasma and aerodynamic force on neutral gas group are considered in the dynamic model.
6) Newton's second law of motion is used to describe the dynamical process of plasma sheet.
7) Effect of mass flow rate in hysteresis ablation was not considered. The total pulse ablation mass is composed of the mass of high speed charged particles generated by ionization and the mass of low speed neutral gas generated by ablation effect
8) The process of accelerating expansion of neutral gas can be regarded as isentropic flow process

2.1. Circuit model

The coaxial PPT circuit can be generally regarded as RLC circuit (as shown in Fig. 2), where the inductance terms L_c, L_{pe} and L_e are due to the capacitor, the electrode geometry and the wires and leads, respectively; the resistance terms R_c、R_e、R_{pe} and R_p are due to the capacitor, the wires and leads, the plate electrodes and the plasma, respectively.

Applying Kirchhoff's law and Faraday's law of electromagnetic induction, the equation is:

$$V_C(t) = V_0 - \frac{1}{C}\int_0^t I(t)dt = IR_T(\mathrm{t}) + \frac{d}{dt}[\lambda_{PPT}(t)] \tag{1}$$

where $R_T(t) = R_c + R_e + R_{pe} + R_p(t)$, $\lambda_{PPT}(t)$ is the magnetic flux through the entire circuit.

$$\lambda_{PPT}(t) = \lambda_c(t) + \lambda_e(t) + \lambda_{pe}(t) = L_cI(t) + L_eI(t) + \iint_{\text{electrodes}} B_{ind}(x, y)\cdot dA \tag{2}$$

where magnetic flux terms $\lambda_c(t)$, $\lambda_e(t)$ and $\lambda_{pe}(t)$ are due to the capacitor, the wires and leads and electrode channel, respectively; B_{ind} and A are the self-induced magnetic field through the plasma sheet and the

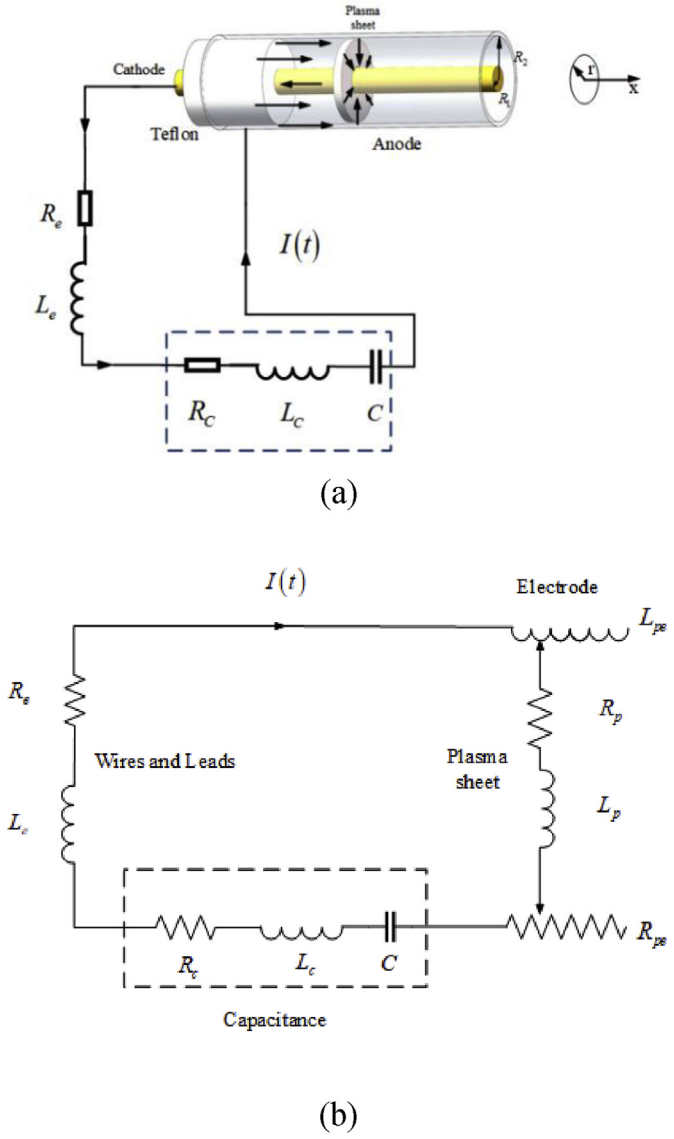

Fig. 2. Circuit of the coaxial PPT.

area vector of the plasma sheet, respectively.

2.2. Magnetic field Model

The current loop composed of the coaxial electrode and plasma sheet can be regarded as spiral wound ring with a rectangular section (as shown in Fig. 3). According to Biot-Savart law and boundary condition of complete conductor, the magnetic field intensity can be written as:

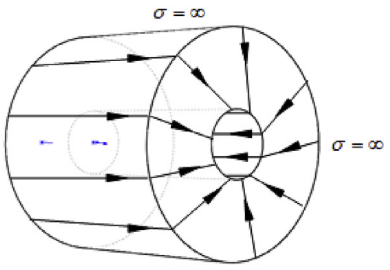

Fig. 3. A spiral wound ring.

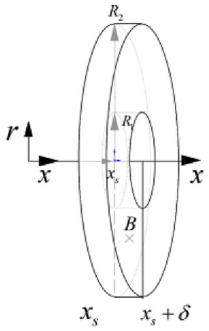

Fig. 4. Plasma sheet.

$$B_{ind} = \mu_0 \frac{I}{2\pi r} \tag{3}$$

Assuming the magnetic field before the current sheet to be equal to zero, as shown in Fig. 4, the complete expression of self-induced magnetic field intensity can be obtained as:

$$B_{ind}(x, r, t) = \begin{cases} \mu_0 \frac{I(t)}{2\pi r}, & 0 < x < x_s(t) \\ \mu_0 \frac{I(t)}{2\pi r}\left[1 - \frac{x - x_s(t)}{\delta}\right], & x_s(t) < x < x_x(t) + \delta \\ 0 & x > x_x(t) + \delta \end{cases} \tag{4}$$

2.3. Inductance model

From the complete expression of self-induced magnetic field, equation (2) can be rewritten as

$$\begin{aligned} \lambda_{PPT}(t) &= L_c I(t) + L_e I(t) + \int_{R_1}^{R_2} \int_{0}^{x_s(t)} \mu_0 \frac{I(t)}{2\pi r} dx d \\ & r + \int_{R_1}^{R_2} \int_{x_s(t)}^{x_s(t)+\delta} \mu_0 \frac{I(t)}{2\pi r}\left[1 - \frac{x - x_s(t)}{\delta}\right] dx dr \\ &= L_c I(t) + L_e I(t) + \left[\mu_0 \frac{x_s(t)}{2\pi} \ln \frac{R_2}{R_1} + \mu_0 \frac{\delta}{4\pi} \ln \frac{R_2}{R_1}\right] I(t) \end{aligned} \tag{5}$$

where μ_0, R_1, R_2, x_s and δ are the vacuum permeability, radius of the cathode electrode, inner radius of the anode electrode and the location and thickness of plasma sheet, respectively.

2.4. Plasma resistance model

Assuming that the plasma is completely ionized, the resistance of the plasma can be regarded as a series of ring resistors of different diameters connected in series (as shown in Fig. 5).

$$R_p = \frac{l}{\delta A} = \int_{R_1}^{R_2} \frac{1}{\sigma_P 2\pi r \delta} dr = \frac{1}{2\pi \sigma_P \delta} \ln \frac{R_2}{R_1} \tag{6}$$

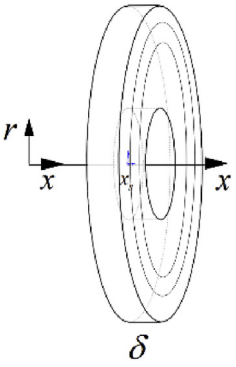

Fig. 5. Plasma resistance model.

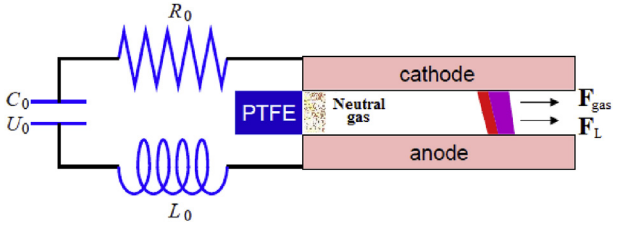

Fig. 6. The dynamics model of coaxial pulsed plasma thruster.

where σ_p is plasma conductivity given by Spitzer-Harm conductivity model [36,37].

The thickness of the current sheet is approximately equal to the diffusion depth of the magnetic field.

$$\delta = \sqrt{\frac{\tau}{\sigma_p \mu_0}} \tag{7}$$

The plasma resistance can be written as,

$$R_p = 8.08 \frac{1}{2\pi T_e^{\frac{3}{4}}} \ln \frac{R_2}{R_1} \sqrt{\frac{\mu_0 \ln\left[1.24 \times 10^7 \left(\frac{T_e^3}{n_e}\right)^{\frac{1}{2}}\right]}{\tau}} \tag{8}$$

where T_e is plasma temperature and n_e is plasma density, and τ is the characteristic pulse time.

2.5. Dynamics model

The thrust of coaxial pulsed plasma thruster is mainly due to magnetic pressure forces and gas dynamic pressure forces (as shown in Fig. 6)

$$\sum F(t) = F_l(t) + F_g(t)$$

where $\sum F(t)$ is the thrust of coaxial pulsed plasma thruster and $F_l(t)$ is Lorentz force acting on a current sheet, and $F_g(t)$ is gas dynamic pressure forces of neutral gas.

Motion of the current sheet is governed by Newton's second law. Assuming the force on the plasma sheet as Lorentz force.

$$\frac{d}{dt}[m_e(t)\dot{x}_s(t)] = F_l(t) = \iiint_{\text{current sheet}} \dot{J} \times B dV = \int_{x_s(t)}^{x_s(t)+\delta} \int_{R_1}^{R_2} \frac{I(t)}{2\pi r \delta} \mu_0 \frac{I(t)}{2\pi r}\left[1 - \frac{x - x_s(t)}{\delta}\right] 2\pi r dr dx = \frac{\mu_0}{4\pi} \ln \frac{R_2}{R_1} [I(t)]^2 \tag{9}$$

Assuming that all the propellant gases are concentrated on the surface of the propellant at $t = 0$, there is no mass accumulation in the acceleration process of the plasma sheet, that is, $m_e(t) = m_0$. Therefore, equation (9) can be rewritten as,

$$F_L(t) = m_0 \ddot{x}_s(t) = \frac{\mu_0}{4\pi} \ln \frac{R_2}{R_1} [I(t)]^2 \tag{10}$$

Impulse bit of the plasma sheet I_{bit}^l:

$$I_{bit}^l(t) = \int_0^t \frac{\mu_0}{4\pi} \ln \frac{R_2}{R_1} [I(t)]^2 d\tau \tag{11}$$

For gas dynamic pressure forces of neutral gas, Guman et al. did some works [34]. The neutral gas mass is accelerated by aerodynamic expansion, as shown in Fig. 7, a schematic diagram of aerodynamic acceleration process. Section 0 is the ablation surface position of the propellant, where the neutral gas group is generated. Section e is the nozzle section of the thruster, from which the accelerated neutral gas is ejected. Since the fluid expands into vacuum the expansion process can be considered isentropic. The acceleration of neutral gas is a process of

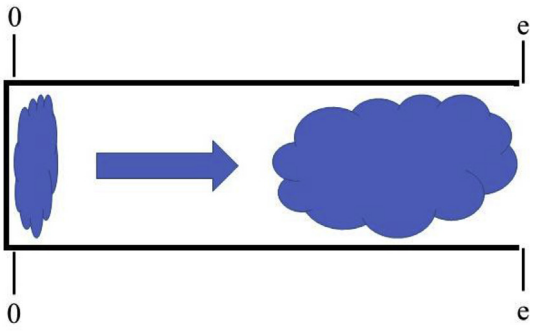

Fig. 7. Acceleration process of neutral gas.

fluid expanding to vacuum, so it is also an isentropic process. Within the spirit of the analysis, it is also reasonable to assume that at any instant the instantaneous mass average flow velocity is equal to the sonic velocity of the expanding fluid element of uniform conditions evaluated at the same instant, that is, u = a*.

Mass flow rate of the neutral gas expanding into the vacuum is thus,

$$dm/dt = V \cdot d\rho/dt = \rho A u = \rho^* A^* a^* \tag{12}$$

where ρ, A, a represent instantaneous density, instantaneous cross-sectional area and instantaneous speed of sound respectively; ρ^*, A^*, a^* are the corresponding critical parameters.

According to the isentropic relation,

$$a = a_0(\rho/\rho_0)^{(\gamma-1)/2} \tag{13}$$

Then, we can get

$$\frac{p}{p_0} = \left(\frac{\rho}{\rho_0}\right)^{\gamma} = \left[1 + \frac{\gamma - 1}{2}\left(\frac{2}{\gamma + 1}\right)^{\frac{\gamma+1}{2(\gamma-1)}} \cdot \frac{a_0 A^*}{V} t\right]^{-\frac{2\gamma}{\gamma-1}} \tag{14}$$

Gas dynamic pressure forces of neutral gas:

$$F_g(t) = \dot{m}_e u_e + (p_e - p_a) A_e \tag{15}$$

External pressure environment of the thruster is vacuum, i. e. $p_a \approx 0$, Combining equation (12) with the isentropic relation, equation (15) can be rewritten as:

$$F_g(t) = \rho^* A^* + \rho^* A^* u^{*2} = p^* A^* (1 + \gamma) \tag{16}$$

Impulse bit of the neutral gas can be written as:

$$I_{bit}^g = \int_0^{\infty} F_g dt = A^* \int_0^{\infty} (\gamma + 1) p^*(t) dt = \frac{2 p_0 V_0}{a_0}\left(\frac{2}{\gamma + 1}\right)^{1/2} \tag{17}$$

where the initial pressure p_0 and speed of sound a_0 are related to the energy added prior to the expansion process. Since relatively large temperature changes occur as a result of energy addition, the initial temperature can be neglected compared to the final fluid temperature. Hence one can write:

$$h + \frac{V^2}{2} = h_0 = \frac{1}{\gamma - 1} a_0^2 \approx \frac{E_g}{m_g} \tag{18}$$

$$a_0 \approx \sqrt{(E_g/m_g)(\gamma - 1)} \tag{19}$$

where m_g is the mass of the neutral gas and E_g is the energy used in the neutral gas flow process, and γ is ratio of specific heats of neutral gas.

For perfect gas,

$$a_0 = \sqrt{\gamma R T}$$
$$p_0 = \rho_0 R T \tag{20}$$

Then,

$$p_0 V_0 = (\gamma - 1) E_g / \gamma \tag{21}$$

According to equations (17), (18) and (21), impulse bit of the neutral gas can be rewritten as [34]:

$$I_{bit}^{g} = \int_0^t F_g(t)d\tau = \left[\frac{8(\gamma-1)}{\gamma^2(\gamma+1)} m_g \cdot E_g\right]^{1/2} \tag{22}$$

2.6. Model solution and performance description

Combined with equations ((1), (5), (8) and (10), the coupled nonlinear integral-differential second-order equations can be written as:

$$\begin{cases} V_0 - \frac{1}{C}\int_0^t I(t)dt = I(t)(R_c + R_e + R_{pe} + R_p) \\ \qquad + \left[L_c + L_e + \mu_0 \frac{x_s(t)}{2\pi} \ln\frac{R_2}{R_1} + \mu_0 \frac{\delta}{4\pi} \ln\frac{R_2}{R_1}\right] \\ \qquad \dot{I}(t) \\ +\mu_0 \frac{x_s(t)}{2\pi} \ln\frac{R_2}{R_1} I(t) \\ m_0 \ddot{x}_s(t) = \frac{\mu_0}{4\pi} \ln\frac{R_2}{R_1} [I(t)]^2 \\ R_p = 8.08 \frac{1}{2\pi T_e^{\frac{3}{4}}} \ln\frac{R_2}{R_1} \sqrt{\frac{\mu_0 \ln\left[1.24\times 10^7 \left(\frac{T_e^3}{n_e}\right)^{\frac{1}{2}}\right]}{\tau}} \end{cases} \tag{23}$$

The initial conditions:

$$x_s(0) = 0,\ \dot{x}_s(0) = 0,\ \int_0^{t=0} I(t)dt = 0,\ I(0) = 0 \tag{24}$$

The terms $x_s(t)$, $I(t)$ are calculated from equations (23) and (24). Then we can get the performance parameters of the thruster.

Specific impulse I_{sp}:

$$I_{sp} = \frac{\dot{x}_e}{g} \tag{25}$$

where $\dot{x}_e$ is the exit velocity of the thruster and g is gravitational acceleration.

Impulse bit I_{bit}:

$$I_{bit} = \int_0^t \sum F(t)d\tau = \int_0^t F_l(t)d\tau + \int_0^t F_g(t)d\tau = \int_0^t \frac{\mu_0}{4\pi} \ln\frac{R_2}{R_1} [I(t)]^2 d\tau + \left[\frac{8(\gamma-1)}{\gamma^2(\gamma+1)} m_g \cdot E_g\right]^{1/2} \tag{26}$$

3. Model validation

3.1. Hardware

We designed a coaxial PPT (shown in Fig. 8). As shown in Fig. 9, the experimental setup consists of the coaxial PPT, a measuring system, a vacuum system and a power supply. The measurement system included an oscilloscope, a high-voltage probe (Tektronix THDP0100), a Rogowski coil (CWT Mini HF 150 R), an electronic balance (Sartorius CPA225D) and an impulse bit measurement system.

In each experiment, the experimental vacuum chamber had a pressure of 5×10^{-3} Pa. The voltages in the coaxial PPT discharge circuits were measured by using a high-voltage probe, and the currents in the circuits were measured by using a Rogowski coil. The total

Fig. 8. Coaxial PPT in experiments.

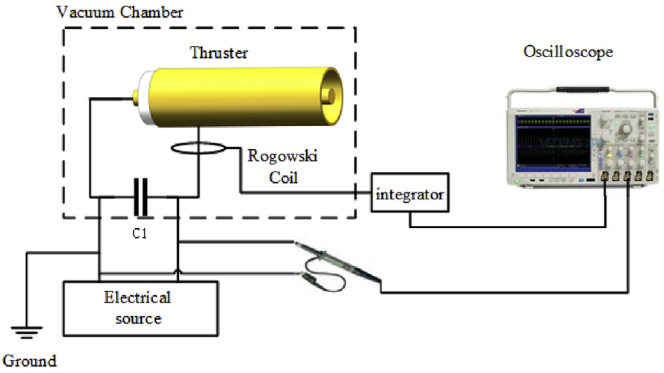

Fig. 9. Experimental system configuration.

ablated mass was measured by using a high-precision balance. In order to ensure the measurement accuracy of the balance, the electronic balance needs to be warmed up for an hour before use and the results on the screen of electronic balance were read after stabilizing for 5 s to reduce the error. In the experiments, to reduce the measurement error, the mass of the PTFE propellant was measured before and after the experiment at least three times in each condition separately and the PTFE propellant block was placed in the atmosphere for an hour before it was weighed after each experiment. Therefore, the difference in average value of the mass of the propellant before and after the experiment is the total mass of ablation for each experimental condition. After hundreds of ignitions, the ablated mass bit could be obtained by using the total mass of ablation divided by the number of successful discharges for each condition. Moreover, to reduce the effects of deposition, the surfaces of the electrodes and propellant were wiped before each test.

Impulse bit of the thruster under different working conditions was measured by using an impulse bit measurement system (shown in Fig. 10). And the parameters of the experimental coaxial PPT are shown in Table 1.

In the experiment, the impulse bit of the thruster is roughly measured by shooting method. A circular sheet is placed at the thruster nozzle. The sheet is suspended by a string. When the thruster works, the high-speed particle flow makes the circular sheet move a certain

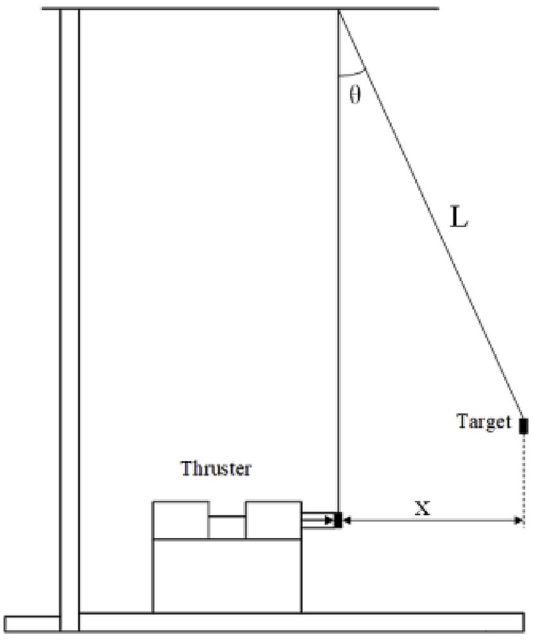

Fig. 10. Measurement of thruster impulse bit.

Table 1
Parameters of the experimental PPT.

Parameters	Values
Capacitance of main capacitor	2 μF
Radius of cathode electrode	0.75 mm
Inner radius of the anode electrode	3 mm
Thickness of the anode electrodes	0.5 mm
Length of electrodes	50 mm

Table 2
Parameters of the impulse bit measurement system.

Parameters	Values
Length of the string (L_s)	0.243 m
Mass of the circular sheet(m_b)	0.1176 g
radius of the circular sheet (r)	4 mm

Table 3
Parameters of the experimental thruster for simulation.

Parameters	Values
Initial Voltage (V)	1500,1300,1000,800
Pulse Ablation Mass (μg)	2.73,1.83,1.13,0.72
Capacitance (μF)	2
Circuit Resistance (mΩ)	100
Circuit Inductance (nH)	130
Acceleration Length (mm)	15
Cathode Radius (mm)	0.75
Anode Radius (mm)	3
Plasma Temperature (eV)	1.5
Electron Density (m-3)	10^{21}

distance. According to the momentum theorem and the law of conservation of energy, the impulse bit measured by the shooting method can be calculated.

$$I_{bit} = Ft = m_b v_b \tag{27}$$

$$\frac{1}{2}mv_b^2 = m_b gL(1-\cos\theta)$$
$$\cos\theta = \sqrt{1-\frac{x^2}{L^2}} \tag{28}$$

Impulse bit I_{bit}:

$$I_{bit} = m_b\sqrt{2gL(1-\cos\theta)} \tag{29}$$

where m_b is the mass of the circular sheet, L is the distance between the suspension point of the string and the center of the circular sheet, x is the horizontal displacement of the circular sheet after a single pulse.

In order to prevent the influence of the plume on the circular sheet, the circular sheet material is made of polyimide. The weight of the circular sheet should be as small as possible so that the moving distance is obvious to reduce the measurement error, but the weight also needs to be kept relatively large relative to the weight of the string. The diameter of the circular sheet is larger than the diameter of the thruster nozzle, ensuring that the sheet can cover the entire plume of the thruster. In the experiment, the motion position of the circular sheet was recorded by camera. The parameters of the impulse bit measurement system are shown in Table 2.

Voltage and current data of the discharge process are measured by experiment and compared with the simulation results to verify the electromechanical model of coaxial pulsed plasma thruster. By using the shooting method, the impulse bit of the thruster can be roughly measured. Then, the impulse bit measured by experiment is compared with the impulse bit estimated by the dynamics model to verify the model.

3.2. Circuit simulation

Some parameters of the experimental thruster for simulation are shown in Table 3.

In Figs. 11–14, the comparisons between experimental data and simulation results at different initial voltages are presented.

From the comparison results, we can see that the model can well simulate the voltage and current changes when the thruster is discharging, and the higher the voltage is, the better the agreement between the model simulation results and the experimental data.

3.3. Impulse bit measurement comparison

The voltage, current and ablative mass data measured by the experiment were put into the model to calculate the impulse bit, and then the calculation result of the model was compared with the value of the impulse bit measured by the experiment (as shown in Table 4 and Fig. 15).

From the result of the impulse bit, we can see that the difference between the experimental results and the calculated results of the model is small, which is in the same order of magnitude range and has

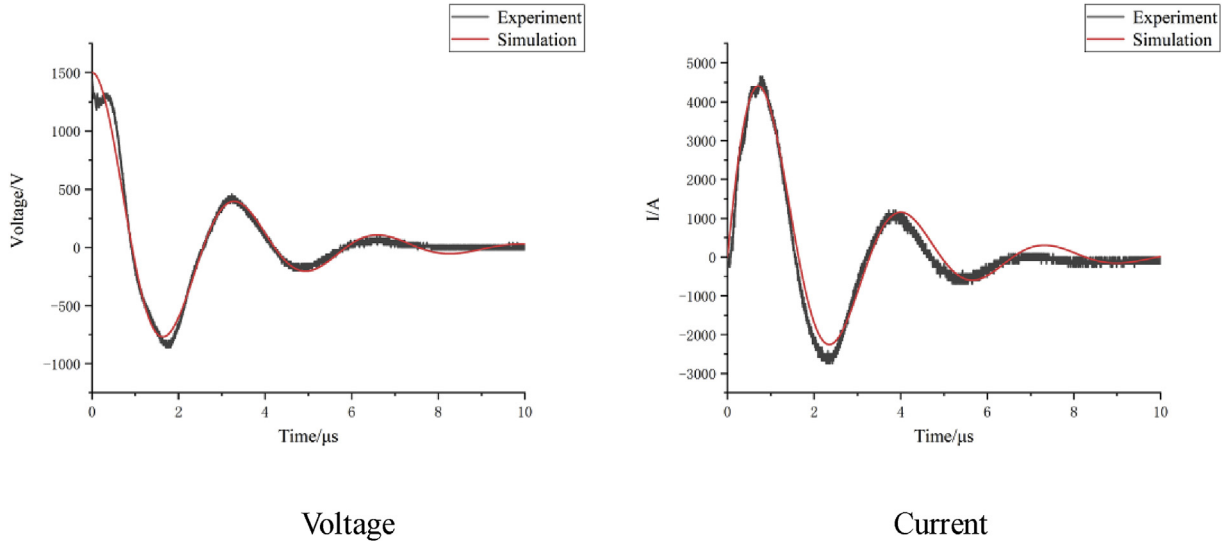

Fig. 11. Initial voltage of 1500 V

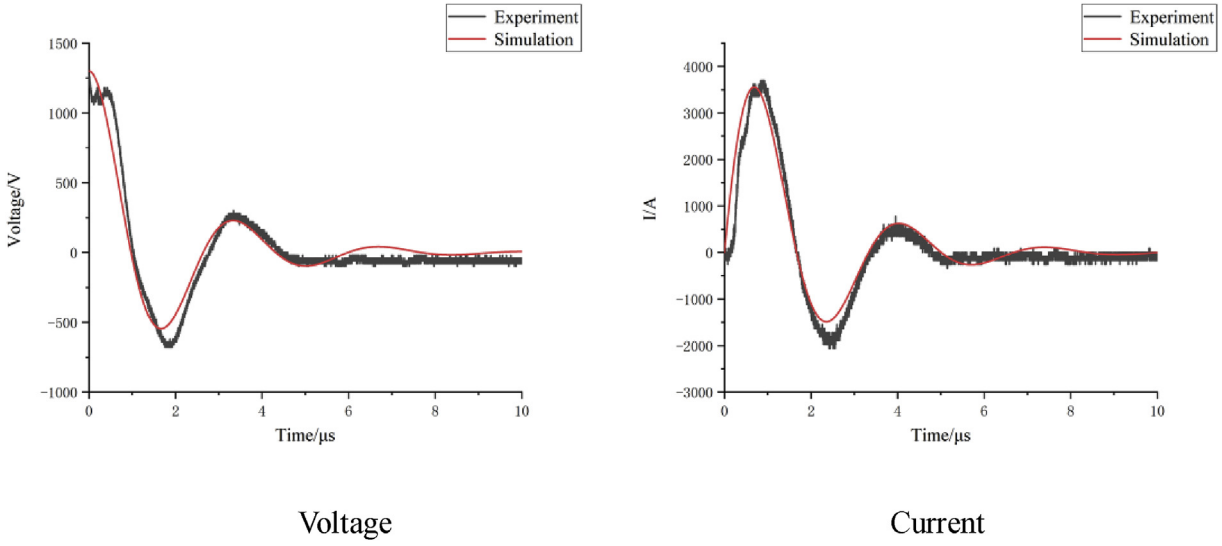

Fig. 12. Initial voltage of 1300 V

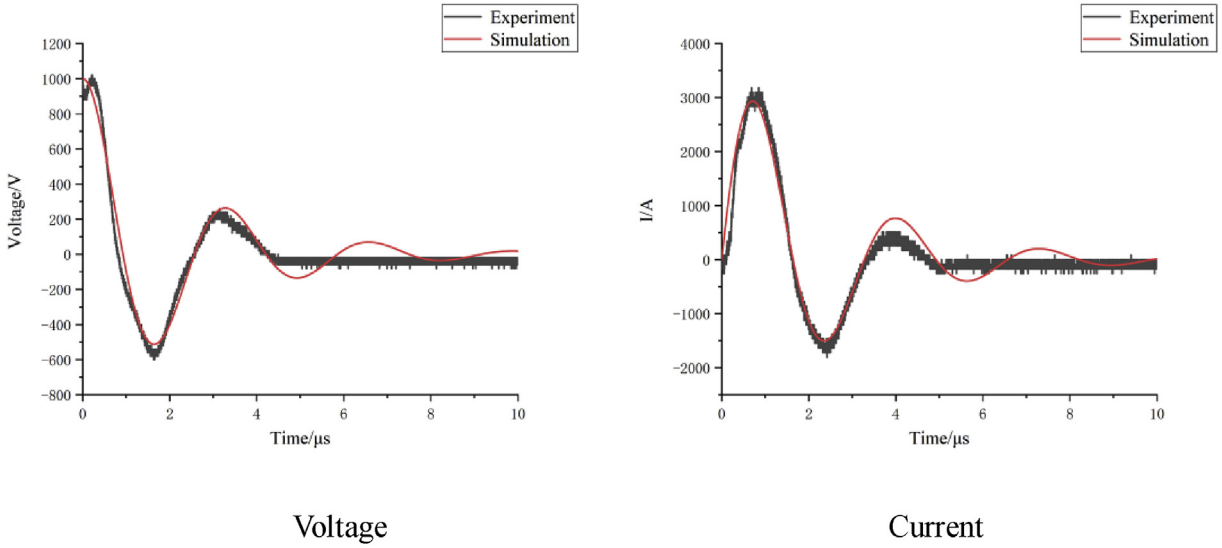

Fig. 13. Initial voltage of 1000 V

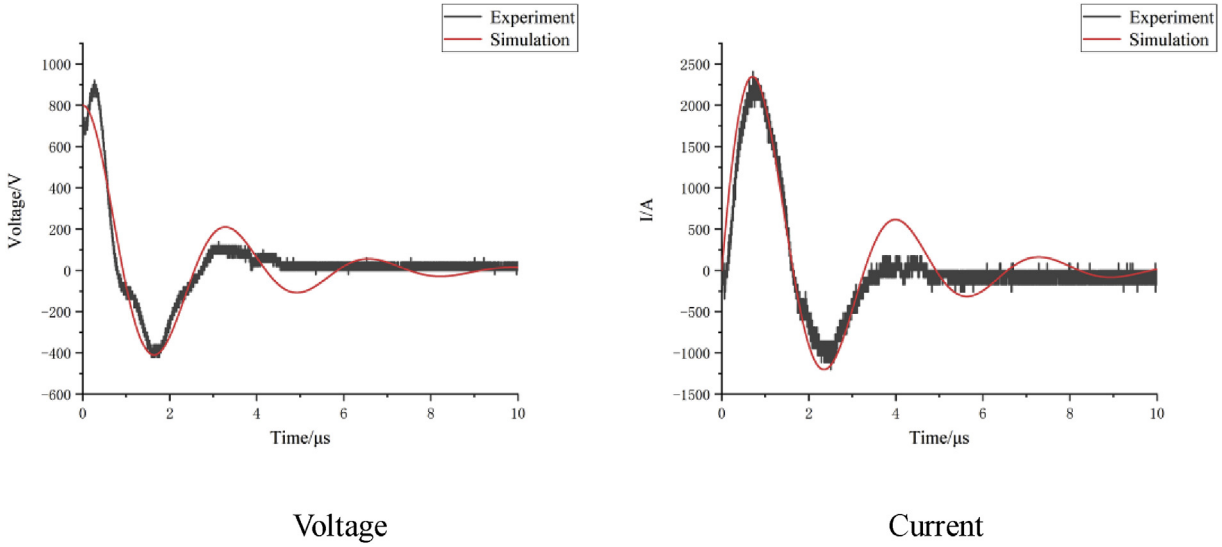

Fig. 14. Initial voltage of 800 V

Table 4
The result of the impulse bit.

Initial Voltage/V	Horizontal distance/m	impulse bit (experiment)/μNs	impulse bit (simulation)/μNs	impulse bit (plasma sheet)/μNs	impulse bit (neutral gas)/μNs
1000 V	$0.0147^{+0.0007}_{-0.0008}$	$10.90^{+0.52}_{-0.60}$	11.43	1.20	10.23
1200 V	$0.0204^{+0.0004}_{-0.0003}$	$15.13^{+0.30}_{-0.23}$	16.73	1.85	14.88
1500 V	$0.0303^{+0.0018}_{-0.0010}$	$22.50^{+1.35}_{-0.75}$	27.72	3.87	23.85

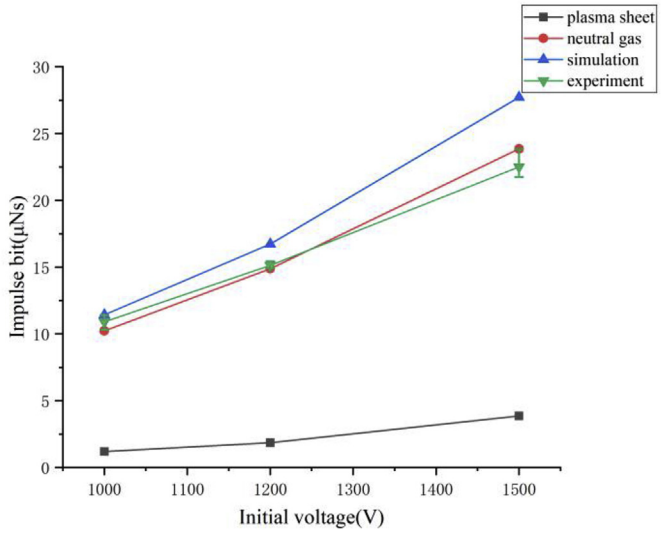

Fig. 15. Comparison of thruster impulse bit.

the same change trend. In the component of the impulse bit, the proportion of electromagnetic impulse bit is very small while, relatively, the impulse proportion of the neutral gas is extremely large.

The deviation between the experimental results and the calculated results of the model come from many sources. The first reason for this deviation is that the experimental result includes errors in the experimental measurement. In this experiment, the center of the circular sheet is taken as the center of mass. Since the mass of the thin string is not negligible relative to the mass of the circular sheet, there are certain errors, and inevitable reading errors also exist in the data post-processing. All of this makes the experimental result lower than the actual value. Second, the model itself. We made a lot of simplifications in the model building process; the result of the calculation is an idealized value, which is larger than the actual value. All of this causes the difference between the experimental results and the calculated value of the model. However, the range of actual values can be estimated through experimental results and model calculation values. Therefore, the impulse bit of the thruster can be roughly estimated by the model established in this paper. So, it can be considered that the impulse bit of the thruster can be preliminarily estimated by the model established in this paper.

4. Conclusion

We compared and verified the model by using the experimental results. The results show that the model established in this paper can well simulate the variation of voltage and current during the working process of coaxial pulsed plasma thruster, and can preliminarily estimate the macro performances of the thruster based on the model. However, we made a lot of simplifications in the model building process. In the model, plasma resistance, plasma temperature and electron density are constant, and propellant ablation process and plasma ablation process are not considered, so there are some deficiencies in the model, which should be identified and addressed with considerations for future improvement.

Declaration of interest statement

The authors declare that there is no conflict of interest between this article and others. The authors declare that they have no known competing financial interests or personal relationships that could have appeared to influence the work reported in this paper.

Acknowledgements

Our research was supported by the National Natural Science Foundation of China (Grant No. 11672039) and the Natural Science Foundation of Shanghai (Grant No.17ZR1413100).

References

[1] Guorui Sun, Zhiwen Wu, Hang Li, Linghan Zeng, Discharge voltage characteristic in ablative pulsed plasma thrusters, Aerospace Sci. Techonol. 86 (2019) 153–159.
[2] Zhiwen Wu, Guorui Sun, Shiyue Yuan, Tiankun Huang, Xiangyang Liu, Kan Xie, Ningfei Wang, Discharge reliability in ablative pulsed plasma thrusters, Acta Astronaut. 137 (2017) 8–14.
[3] Zhiwen Wu, Guorui Sun, Tiankun Huang, Xiangyang Liu, Kan Xie, Ningfei Wang, Optimization of the energy distribution in ablative pulsed plasma thrusters, AIAA J. (2018) 1–11.
[4] S. Ciaralli, M. Coletti, S.B. Gabriel, Results of the qualification test campaign of a pulsed plasma thruster for cubesat propulsion (PPTCUP), Acta Astronaut. 121 (2016) 314–322.
[5] Armen Poghosyan, Alessandro Golkar, CubeSat evolution: analyzing CubeSat capabilities for conducting science missions, Prog. Aerosp. Sci. 88 (2017) 59–83.
[6] Giancarlo Santilli, et al., CubeSat constellations for disaster management in remote areas, Acta Astronaut. 145 (2018) 11–17.
[7] S. Ciaralli, M. Coletti, S.B. Gabriel, Results of the qualification test campaign of a pulsed plasma thruster for cubesat propulsion (PPTCUP), Acta Astronaut. 121 (2016) 314–322.
[8] W.A. Hoskins, C. Rayburn, C. Sarmiento, Pulsed plasma thruster electromagnetic compatibility: history, theory, and the flight validation on EO-1, 39th AIAA/ASME/SAE/ASEE Joint Propulsion Conference, AIAA, Huntsville, AL, USA, July 20032003-5016.
[9] M.V. Silnikov, K.S. Kulakov, S.L. Kulakov, D.V. Panov, Correction thruster development based on high-current surface discharge in vacuum, Acta Astronaut. 109 (2015) 177–181.
[10] V. Zhurin, A. Porotnikov, V. Shadov, Electric propulsion research and development in the USSR, 12th International Electric Propulsion Conference, 1976.
[11] M. Keidar, I.D. Boyd, E.L. Antonsen, et al., Optimization issues for a micro pulsed plasma thruster, J. Propuls. Power 22 (1) (2006) 48–55.
[12] Yongjie Ding, Wuji Peng, Wei Liqiu, Guoshun Sun, Li Hong, Daren Yu, Computer simulations of Hall thrusters without wall losses designed using two permanent magnetic rings, J. Phys. D Appl. Phys. 49 (46) (2016) 465001.
[13] Yongjie Ding, Hezhi Sun, Wei Liqiu, Li Peng, Hongbo Su, Wuji Peng, Daren Yu, A 200 W Hall thruster with hollow indented anode, Acta Astronaut. 139 (2017) 521–527.
[14] Yongjie Ding, Wuji Peng, Hezhi Sun, Wei Liqiu, Ming Zeng, Fufeng Wang, Daren Yu, Performance characteristics of No-Wall-Losses Hall thruster, Eur. Phys. J. Spec. Top. 226 (2017) 2945–2953.
[15] Yongjie Ding, Wuji Peng, Hezhi Sun, Wei Liqiu, Ming Zeng, Fufeng Wang, Daren Yu, Visual evidence of suppressing the ion and electron energy loss on the wall in Hall thrusters, Jpn. J. Appl. Phys. 56 (3) (2017) 038001.
[16] Yuichi Nakagawa, Hiroyuki Koizumi, Hiroki Kawahara, Kimiya Komurasaki, Performance characterization of a miniature microwave discharge ion thruster operated with water, Acta Astronaut. 157 (2019) 294–299.
[17] K. Xie, Q. Xia, J.D. Williams, et al., Extracted current, bias voltage, and ion production of cathodic hollow-cathode-driven plasma contactors, J. Spacecr. Rocket. 52 (4) (2015) 1181–1192.
[18] Michael Keidar, Taisen Zhuang, Alexey Shashurin, et al., Micro-Cathode Arc thruster for small satellite propulsion, 53rd AIAA Aerospace Sciences Meeting, AIAA SciTech Forum, Kissimmee, Florida, 2015.
[19] Zhiwen Wu, Guorui Sun, Continuous discharge in micro ablative pulsed plasma thrusters, Acta Astronaut. 149 (2018) 11–14.
[20] Guorui Sun, Zhiwen Wu, Ignition mechanism in ablative pulsed plasma thrusters with coaxial semiconductor spark plugs, Acta Astronaut. 151 (2018) 120–124.
[21] Kimiya Komurasaki, Yoshihiro Arakawa, Performance calculation of Hall thrusters,

Acta Astronaut. 38 (1996) 185–192.
[22] H.K. Cho, J. Rhee, Development of Hall thruster propulsion system for stsat-3 application, Acta Astronaut. 72 (2012) 90–97.
[23] Junichiro Aoyagi, et al., Total impulse improvement of coaxial pulsed plasma thruster for small satellite, Vacuum 83 (1) (2008) 72–76.
[24] Jeremy J. Selstrom, Thrust and Performance Study of Micro Pulsed Plasma Thrusters, No. AFIT/GAE/ENY/10-M21, Air Force Inst of Tech Wright-Patterson Afb oh School of Engineering and Management, 2010.
[25] Lee I. Watson, Using a Gatling-Gun Configured Micro Pulsed Plasma Thruster as a Means to Control Micro Satellites with Extreme Precision, (2011).
[26] L. Zeng, Z. Wu, G. Sun, T. Huang, K. Xie, N. Wang, A new ablation model for ablative pulsed plasma thrusters, Acta Astronaut. 160 (2019) 317–322.
[27] T.R. Nada, One-dimensional model of a pulsed plasma thruster, Aeronaut. J. 117 (1195) (2013) 929–942.
[28] Robert G. Jahn, F.A. Lyman, Phys. Electr. Propul. (1969) 655-655.
[29] Peter Michael Waltz, Analysis of a Pulsed Electromagnetic Plasma Thruster, Diss (1969).
[30] R.J. Leiweke, An advanced pulsed plasma thruster design study using one-dimensional slug modeling, AFOSR Summer Research Program Final Report, Phillips Laboratory, Kirkland Air Force Base, New Mexico, 1996.
[31] Nikolaos Gatsonis, Michael Demetriou, Prospects of plasma flow modeling and control for micro pulsed plasma thrusters, 40th AIAA/ASME/SAE/ASEE Joint Propulsion Conference and Exhibit, 2004.
[32] David Laperriere, N. Gatsonis, M. Demetriou, Electromechanical modeling of applied field micro pulsed plasma thrusters, Aiaa/asme/sae/asee Joint Propulsion Conference & Exhibit, 2005.
[33] Henri Wagner, Monika Auweter-Kurtz, Slug model and snowplow model for pulsed plasma thruster description, 40th AIAA/ASME/SAE/ASEE Joint Propulsion Conference and Exhibit, 2004.
[34] William J. Guman, Pulsed Plasma Technology in Microthrusters, No. PCD-TR-68-14, Fairchild Hiller Corp Farmingdale Ny Republic Aviation Div, 1968.
[35] V.F. Nikitin, N.N. Smirnov, M.N. Smirnova, et al., On board electronic devices safety subject to high frequency electromagnetic radiation effects, Acta Astronaut. 135 (2017) 181–186.
[36] M. Mitchner, C.H. Kruger, Partially Ionized Gases Chapter 2 (1973) Indianapolis.
[37] A.H. Haus, J.R. Melcher, Electromagnetic Fields and Energy vols. 8 and 10, Prentice-Hall, Englewood Cliffs, New Jersey, 1989 Chapters 1.